Inhibition of proteasome deubiquitinating activity as a novel cancer therapy

D'Arcy, Pádraig; Brnjic, Slavica; Hägg Olofsson, Maria; Fryknäs, Mårten; Lindsten, Kristina; De Cesare, Michelandrea; Perego, Paola; Sadeghi, Behnam; Hassan, Moustapha; Larsson, Rolf; Linder, Stig

Inhibition of proteasome deubiquitinating activity as a novel cancer therapy

Pádraig D'Arcy[1], Slavica Brnjic[1], Maria Hägg Olofsson[1], Mårten Fryknäs[2], Kristina Lindsten[3], Michelandrea De Cesare[4], Paola Perego[4], Behnam Sadeghi[5], Moustapha Hassan[6], Rolf Larsson[2] and Stig Linder[1]

[1]Department of Oncology & Pathology, Karolinska Institute, 171 76 Stockholm, Sweden, [2]Division of Clinical Pharmacology, Department of Medical Sciences, Uppsala University Hospital, 751 85 Uppsala, Sweden, [3]Department of Cell & Molecular Biology, Karolinska Institute, 171 77 Stockholm, Sweden, [4]Fondazione IRCCS, Istituto Nazionale per Studio e Cura dei Tumori, 20133 Milan, Italy, [5]Experimental Cancer Medicine, Institution for Laboratory Medicine, Karolinska Institutet, 141 86 Stockholm, Sweden, [6]Clinical Research Center Novum, Karolinska University Hospital Huddinge, 141 86 Stockholm, Sweden.

P.D. and S.B. contributed equally to this work.

Running title: Inhibition of proteasome deubiquitinating activity

Key words: Cancer therapy, apoptosis, proteasome, deubiquitinating enzymes, USP14, UCHL5

Correspondence and requests for materials should be addressed to S.L. (Stig.Linder@ki.se)

ABSTRACT

Ubiquitin-tagged substrates are degraded by the 26S proteasome; a multi-subunit complex comprising a proteolytic 20S core particle (20S CP) capped by 19S regulatory particles (19S RP) [1,2]. The approval of bortezomib for the treatment of multiple myeloma has validated the 20S CP as an anti-cancer drug target [3]. Here, we describe the small molecule b-AP15 as a novel class of proteasome inhibitor that abrogates the deubiquitinating (DUB) activity of the 19S RP. b-AP15 inhibited the activity of two 19S RP-associated DUBs, ubiquitin carboxyl-terminal hydrolase 5 (UCHL5) and ubiquitin specific peptidase 14 (USP14), resulting in accumulation of polyubiquitin. b-AP15 induced tumor cell apoptosis insensitive to *TP53* status and over-expression of the apoptotic inhibitor *Bcl-2*. We show that treatment with b-AP15 inhibited tumor progression in four different *in vivo* solid tumor models and inhibited organ infiltration in an acute myeloid leukemia (AML) model. Our results show that the DUB activity of the 19S RP is a novel anti-cancer drug target.

We identified b-AP15 (**Fig. 1a**) in a screen for compounds that induce the lysosomal apoptosis pathway [4,5]. To characterize the connection between b-AP15 and other anti-cancer drugs we compared the gene expression signature of b-AP15- treated cells to a collection of expression signatures for >1300 bioactive compounds in the CMAP database (www.broad.mit.edu/cmap) [6]. b-AP15 induced a gene expression profile similar to that of several well characterized proteasome inhibitors [7-10] (**Fig. 1b, Supplementary Spreadsheet**). To test whether b-AP15 blocked cellular proteasome function we utilized a reporter cell line expressing ubiquitin tagged to yellow fluorescent protein (Ub^{G76V}-YFP) that is constitutively targeted for proteasomal degradation [11]. We observed a dose-dependent accumulation of the Ub^{G76V}-YFP reporter (IC_{50}=0.8 μM), indicating impaired proteasome degradation (**Fig. 1c**). Defects in ubiquitin turnover are a characteristic of proteasome inhibition [12]. We indeed observed rapid accumulation of polyubiquitin in b-AP15-treated colon carcinoma HCT-116 cells, with a similar kinetic but higher molecular weight than that of the 20S CP inhibitor bortezomib, suggesting inhibition of the ubiquitin-proteasome system (UPS) (**Fig. 1d**). The UPS controls the turnover of many cell cycle regulatory proteins including inhibitors of the cyclin-dependent kinases, CDKN1A, CDKNIB and the tumor suppressor TP53 [13-15]. Treatment with b-AP15 increased the levels of all three in a dose-dependent manner (**Fig. 1e**), without altering the levels of ornithine decarboxylase 1 (ODC1), an ubiquitin-independent proteasome substrate [16] (**Fig. 1f**). Consistent with the accumulation of cell cycle inhibitors, we observed G2/M phase cell cycle arrest (**Fig. 1g**). Cell cycle arrest was not associated with increased levels of DNA damage markers such as p-p53 [17] or p-H2AX [18] suggesting that b-AP15 is non-genotoxic (**Supplementary Fig. 1**).

b-AP15 treatment increased the number of hypodiploid cells (**Fig. 1g**) and was associated with increased levels of apoptotic markers, including activated caspase-3, caspase-cleaved poly-ADP ribose polymerase (PARP) (**Fig. 1e**) and cytokeratin-18 (CK18) (**Supplementary Fig. 2a**). Apoptosis and decreased cell viability (**Supplementary Fig. 2b**) was observed at drug concentrations that induced polyubiquitin accumulation; thus providing a link between proteasome inhibition and cytotoxicity. Notably we found that b-AP15 was more toxic to HCT-116 cells compared to immortalized epithelial cells (hTERT-RPE1) or peripheral blood mononuclear cells (PBMC) (**Supplementary Fig. 2c,d**). These differences were larger than those observed for bortezomib (**Supplementary Fig. 2e,f**). Bortezomib-induced apoptosis is sensitive to *TP53* status and the expression levels of the anti-apoptotic *Bcl-2* oncogene [19,20]. Using isogenic clones of HCT-116, we found that b-AP15 induced apoptosis which was insensitive to over-expression of *Bcl-2* and disruption of *TP53,* as well as *BAX* and *BBC3*, mediators of the mitochondrial apoptotic pathway (**Fig. 1h, Supplementary Fig. 3**).

We next attempted to define how b-AP15 inhibited proteasome activity *in vitro*. We observed no inhibition of any of the proteolytic activities of the proteasome (**Supplementary Fig. 4**), no disassociation of the proteasome or inhibition of ubiquitin binding (**Supplementary Fig. 5**). The chemical structure of b-AP15 contains a α-ß dienone with two sterically accessible ß-carbons (**Fig. 1a**). A similar pharmacophore was previously described in DUB inhibitors [21]. However, when we tested cellular DUB activity using ubiquitin 7-amido-4-methylcoumarin (Ub-AMC) on b-AP15-treated cells we observed no reduction in total DUB activity (**Supplementary Fig. 6**). Given the similarities in pharmacophore structure and our previous data showing that b-AP15 inhibits proteasome activity independently of the

20S CP, we hypothesized that b-AP15 may inhibit the proteasome indirectly, by blocking the de-ubiquitinating activity of the 19S RP necessary for efficient proteasome degradation. *In vitro* assays using purified 19S RP or 26S proteasomes confirmed that b-AP15 inhibited deubiquitinating activity using a variety of substrates including Ub-AMC (**Fig. 2a**), Ub-GFP [22] (**Fig. 2b,c)** ubiquitinated HDM2 (**Fig. 2d**) and K48- and K63-linked ubiquitin tetramer chains (**Fig. 2e**). This inhibition of chain disassembly may account for the accumulation of high molecular weight ubiquitin conjugates observed in b-AP15 treated cells (**Fig. 1d,e**).

The deubiquitinating activity of the proteasome is attributed to the action of three DUBs, UCHL5, USP14 and POH1 all localized within the 19S RP [23-25]. UCHL5 and USP14 are sensitive to N-ethylmaleimide (NEM), a general inhibitor of cysteine proteases, whereas POH1 in contrast is sensitive to the metal chelator N,N,N,N-Tetrakis-(2-pyridylmethyl)ethylenediamine (TPEN) [26]. Residual DUB activity was still present after co-treatment of 19S RP with NEM and b-AP15 (**Fig. 3a**), but abolished upon co-treatment of 19S RP with b-AP15 and TPEN (**Fig. 3b**), suggesting that b-AP15 primarily inhibits one or both of the NEM-sensitive cysteine DUBs. The β-carbons in b-AP15 may serve as Michael acceptor moieties conferring covalent binding to cysteine residues in target proteins. However our *in vitro* assays showed that b-AP15 is a reversible inhibitor (**Supplementary Fig. 7a–c**) and that glutathione does preclude its inhibitory activity (**Supplementary Fig. 7d**).

To identify which DUBs were inhibited by b-AP15, we performed competitive labeling experiments using hemagglutinin tagged ubiquitin vinylsulphonone (HA-UbVS), an active site directed probe that irreversibly reacts with cysteine DUBs [23]. Incubation of 19S RP or 26S proteasomes with b-AP15 abolished Ub-VS labeling of

two DUBs of molecular weights corresponding to UCHL5 and USP14 (**Fig. 3c**). We observed a similar result using UbVS on lysates derived from drug-treated cells. Immunoblot analysis showed a downward shift in the molecular weight of both USP14 and UCHL5 due to a loss of activity and decreased UbVS labeling (**Fig. 3d**). We also observed reduced DUB activity in affinity-purified proteasomes, but not in cell lysates, from b-AP15-treated cells. (**Supplementary Fig. 8a**). Consistent with the notion that b-AP15 is not a general DUB inhibitor, we observed minimal inhibition on recombinant and cytosolic non-proteasomal cysteine DUBs (**Supplementary Fig. 8b,c**).

We next investigated the effect of b-AP15 on tumor growth *in vivo.* When b-AP15 was administered daily to SCID mice bearing FaDu squamous carcinoma xenografts, we observed significant antitumor activity (treated/control tumor volume, T/C=0.4, P=<0.001) (**Fig. 4a**). When we analyzed tumor death by measuring xenograft-derived CK18 in circulation [27,28], we observed a significant increase in the plasma levels of total CK18 (P=0.01) along with increased levels of caspase-cleaved CK18 (CK18-Asp396) (**Fig. 4b**), showing that b-AP15 has activity against tumor cells *in vivo*. We also examined disease-free survival in *Bcl-2* over-expressing HCT-116 colon carcinoma xenografts. b-AP15 treatment significantly delayed tumor onset in comparison to vehicle-treated control with 2 out of 6 of the treated mice being completely disease free at the end of the study (P= 0.0136 by log rank test) (**Fig. 4c**).

Similarly, b-AP15 inhibited tumor growth in syngenic mice models using less frequent administration schedules. We administered b-AP15 to C57BL/6J mice bearing lung carcinomas (LLC) using a 2 day on/2 day off schedule and to BALB/c mice bearing orthotopic breast carcinoma (4T1) using a 1 day on/3 day off schedule.

b-AP15 significantly inhibited tumor growth in both models with a tumor volume response of T/C=0.16, (P=<0.01) and T/C=0.25 (P=<0.001), respectively (**Fig. 4d,e**). We also observed a reduction in the number of pulmonary metastases in the b-AP15-treated group of 4T1 breast carcinoma (Fig. 4f). Importantly, we observed no change in animal behavior or loss in body weight (**Supplementary Fig. 9**).

Since our previous data showed that b-AP15 promoted the accumulation of polyubiquitin and inhibited cleavage of K48-linked ubiquitin chains (**Fig. 1c,2c**), we tested the effect of b-AP15 on the UPS activity *in vivo* by staining tumor sections with antibodies to K48-linked polyubiquitin chains. High levels of K48-linked polyubiquitin accompanied by caspase-3 activation were observed in the b-AP15-treated group, confirming inhibition of DUB activity (**Fig. 4g**).

Next, we investigated the effect of b-AP15 on tumor cell invasion in an aggressive leukemic model (AML). We administered b-AP15 (daily from d 8 to d 14) to C57BL/6J mice bearing C1498 leukemia. Leukemia regression was observed in eight out of ten b-AP15-treated mice (P=<0.001) compared to vehicle treated animals (n=10). Liver from control animals showed hepatomegaly and massive invasion of myeloid leukemic cells into liver tissue (**Fig. 4h**). In contrast, b-AP15-treated mice showed normal structured hepatocytes and lower levels of leukemic blast infiltration. Ovary tissue of control mice also showed massive invasion of leukemic blasts and interstitial bleeding, not evident in the treated group. Taken together, our results demonstrate that b-AP15 inhibits tumor growth *in vivo*.

Ubiquitin C-terminal hydrolases and ubiquitin specific peptidases are major subgroups of the approximately one hundred DUBs encoded by the human genome [29].

The reason for specificity of b-AP15 for UCHL5 and USP14 in the 19S RP may be related to unique conformations of these enzymes in the 19S RP or due to drug-induced alterations of the 19S RP structure. Interestingly, a specific inhibitor of proteasome bound USP14 was recently described [30]. Treatment of cells with this inhibitor resulted in enhanced degradation of proteasome substrates. Taken together, these different results suggest a degree of redundancy between USP14 and UCHL5 with regard to ubiquitin disassembly so that cells tolerate the loss of one DUB enzyme but not both. Indeed it has been reported that loss of both UCHL5 and USP14 (but not either alone) leads to the accumulation of polyubiquitinated proteins and inhibition of protein degradation without altering the structure or catalytic capabilities of the proteasome [31], similar to the phenotype observed following b-AP15- treatment. Strong expression of chaperone genes was observed in b-AP15-treated cells (**Supplementary Table 1,2**), showing induction of a proteotoxic response. These findings raise the possibility that high molecular weight ubiquitin-substrate complexes accumulating as a result of DUB inhibition generate strong cytotoxicity.

We conclude that the DUB activity of the 19S RP is a promising target for cancer treatment. The cellular response to b-AP15 is not only distinct to that of bortezomib with regard to involvement of apoptosis regulators, but also with regard to the sensitivity of tumor cell lines in the NCI-60 cell line panel (http://dtp.nci.nih.gov) with colon carcinoma and CNS tumor cell lines being most sensitive (**Supplementary Fig. 10**). If proven to be effective in the treatment of human malignancies, inhibitors of 19S RP DUB activity may display a different therapeutic spectrum than inhibitors of 20S enzymatic activity thereby adding to the arsenal of available therapy options.

Acknowledgements: We wish to thank M. Glickman (Department of Biology, Technion-Israel Institute of Technology) for providing the Ub-GFP constructs, N. Dantuma (Department of Cell and Molecular Biology, Karolinska Institutet) for providing the MelJuSo Ub-YFP reporter cell line, B. Vogelstein (Sidney Kimmel Comprehensive Cancer Center, John Hopkins University) for providing the HCT-116 cell lines with targeted disruptions, L. Perup Segerström for technical advice and L. Gatti for drug formulation. We thank Cancerfonden, Radiumhemmets forskningsfonder, Vetenskapsrådet, Strategiska forskningsstiftelsen, Vinnova, European Union CHEMORES, FP 6 (LSHC-CT-2007-037665) and Swedish Children Cancer Society for support.

Author Contributions: All authors were involved in designing experiments and interpreting data. P.D. and S.B. carried out most of the experiments and contributed equally to this work. P.D. and S.L. wrote the manuscript. M.H.O performed the immunohistochemisty. M.F. and R.L performed the CMAP analysis and *in vitro* cytotoxicity analysis. K.L. performed DUB labeling. M.D. and P.P. performed the *in vivo* study on colon carcinoma xenografts. B.S. and M.H performed the *in vivo* study and staining on the AML model.

Figure 1: b-AP15 inhibits the ubiquitin-proteasome system. (**a**) Chemical structure of b-AP15 (3,5-bis[(4-nitrophenyl)methylidene]-1-prop-2-enoylpiperidin-4-one). (**b**) Connectivity map of b-AP15 treated MCF7 cells. The top 5 compounds that induce a gene expression profile similar to b-AP15 are listed. (**c**) b-AP15 inhibits degradation of ubiquitin-tagged YFP in a proteasome reporter cell line. Levels of Ub^{G76V}-YFP accumulation was determined by flow cytometry and immunoblotting. (**d**) Immunoblot of ubiquitin conjugation in HCT-116 cells treated with b-AP15 (1 μM) or bortezomib (100 nM). (**e**) Immunoblot of ubiquitin conjugates, caspase 3 activation PARP cleavage, TP53, CDKN1A and CDKN1B in HCT-116 cells following 24 h treatment with the indicated concentrations of b-AP15. (**f**) Immunoblot of ODC-1 levels in HCT-116 cells following treatment with bortezomib (100 nM) or b-AP15 (1 μM). Values represent quantified optical density units of ODC-1 normalized to ß-actin. (**g**) Cell cycle profiles of b-AP15 treated HCT-116 cells. Cells were analyzed by propidium iodide staining and flow cytometry. (**h**) Levels of caspase activity in isogenic HCT-116 cells as determined by ELISA for caspase cleaved cytokeratin-18 (CK18-Asp396) following treatment with bortezomib (100 nM) or b-AP15 (1 μM) (**'P=0.01, ***'P=0.001).

Figure 2: b-AP15 inhibits deubiquitination by the 19S RP. (**a**) Inhibition of Ub-AMC cleavage by 19S RP and 26S proteasomes following treatment with b-AP15. Ubiquitin aldehyde (Ubal), a general DUB inhibitor is included as a control. (**b**) Immunoblot of 19S RP mediated cleavage of Ub-GFP. 19S RP were pre-treated with DMSO or indicated concentrations of b-AP15 followed by addition of recombinant Ub-GFP as a DUB substrate. (**c**) Kinetic of 19S RP Ub-GFP cleavage following b-

AP15 treatment. (**d**) b-AP15 inhibits de-ubiquitination of Hdm2. Ubiquitinated Hdm2 was added to DMSO or b-AP15 (50 μM) treated 19S RP followed by immunoblotting. (**e**) Ubiquitin chain disassembly reactions of K63/K48 linked ubiquitin tetramers by 19S RP following treatment with DMSO or b-AP15 (50 μM).

Figure 3: b-AP15 inhibits the 19S RP DUBs UCHL5 and USP14. (**a**) 19S RP were pre-treated with DMSO, NEM (10 mM), b-AP15 (50 μM) or **b,** TPEN (250 μM) followed by addition of Ub-GFP followed by immunoblotting with anti GFP antibodies. (**c**) Active site directed labeling of proteasomal. DUBs. Purified 19S or 26S proteasomes were pre-treated with DMSO, NEM or b-AP15 followed by labeling with HA-UbVS and immunoblotting. (**d**) Immunoblot of HCT-116 cells treated with b-AP15 (1 μM) for 3 h. DUBs from whole cell lysates were labeled with HA-UbVS followed by SDS-PAGE and immunoblotting with indicated antibodies.

Figure 4: b-AP15 inhibits tumor growth *in vivo*. (**a**) SCID mice bearing FaDu human tumor xenografts were treated by daily subcutaneous injection with either vehicle (n =10) or 5 mg kg^{-1} b-AP15 (n=15). Mean tumor volume ± SEM are shown. (***P=<0.001). (**b**) Total levels of tumor derived CK18 and caspase cleaved (CK18-Asp396) in circulation following b-AP15 treatment (**P=0.01). (**c**) Disease free survival of nude mice challenged with HCT-116 *Bcl-2*$^{+}$ cells. Mice were treated with vehicle (n=6) or 5 mg kg^{-1} b-AP15 (n=6) 4–5 times weekly for 3 weeks and monitored for tumor onset. (log-rank, P=0.0136, hazard ratio = 7.9). (**d**) C57BL/6J mice bearing syngenic lung carcinoma (LLC) tumors were treated with either vehicle (n = 4) or 5 mg kg^{-1} b-AP15 (n=4) in a 1 day on/2 day off cycle. Mean tumor volume ± SEM are shown. (**P=<0.01). (**e**) BALB/c mice bearing orthotopic breast carcinomas (4T1) were treated with either vehicle (n =5) or 2.5 mg kg^{-1} b-AP15 (n=5) in a 1 day on/3 day off cycle. Mean tumor volume ± SEM are shown. (**P=<0.01).

(**f**) Box and whisker plots of pulmonary metastatic colonies from vehicle or b-AP15 treated 4T1 breast carcinomas. Boxes represent the upper and lower quartiles and median, whiskers show maximum and minimum values. (**g**) Representative immunohistochemical staining for K48-linked ubiquitin accumulation and cleaved caspase-3 in vehicle and b-AP15 treated 4T1 tumors (scale bars, 20 μm). (**h**) AML infiltration in liver and ovary of vehicle or treated mice. Liver of vehicle treated mice showed invasion of leukemic blasts along with glycogen depletion and non-specific hemorrhage. Ovary section of vehicle treated mouse showing massive invasion of leukemic blasts and interstitial bleeding. In contrast ovary from showed few infiltrated blasts and normal morphology (scale bars, 250 μm).

1. Rechsteiner, M., Hoffman, L. & Dubiel, W. The multicatalytic and 26 S proteases. *J Biol Chem* **268**, 6065-6068 (1993).
2. Chu-Ping, M., Vu, J.H., Proske, R.J., Slaughter, C.A. & DeMartino, G.N. Identification, purification, and characterization of a high molecular weight, ATP-dependent activator (PA700) of the 20 S proteasome. *J Biol Chem* **269**, 3539-3547 (1994).
3. Adams, J. & Kauffman, M. Development of the proteasome inhibitor Velcade (Bortezomib). *Cancer Invest* **22**, 304-311 (2004).
4. Berndtsson, M.*, et al.* Induction of the lysosomal apoptosis pathway by inhibitors of the ubiquitin-proteasome system. *Int J Cancer* **124**, 1463-1469 (2009).
5. Erdal, H.*, et al.* Induction of lysosomal membrane permeabilization by compounds that activate p53-independent apoptosis. *Proc Natl Acad Sci U S A* **102**, 192-197 (2005).
6. Lamb, J.*, et al.* The Connectivity Map: using gene-expression signatures to connect small molecules, genes, and disease. *Science* **313**, 1929-1935 (2006).
7. Adams, J.*, et al.* Potent and selective inhibitors of the proteasome: dipeptidyl boronic acids. *Bioorg Med Chem Lett* **8**, 333-338 (1998).
8. Shibata, T.*, et al.* An endogenous electrophile that modulates the regulatory mechanism of protein turnover: inhibitory effects of 15-deoxy-Delta 12,14-prostaglandin J2 on proteasome. *Biochemistry* **42**, 13960-13968 (2003).
9. Yang, H., Chen, D., Cui, Q.C., Yuan, X. & Dou, Q.P. Celastrol, a triterpene extracted from the Chinese "Thunder of God Vine," is a potent proteasome inhibitor and suppresses human prostate cancer growth in nude mice. *Cancer Res* **66**, 4758-4765 (2006).
10. Yang, H., Shi, G. & Dou, Q.P. The tumor proteasome is a primary target for the natural anticancer compound Withaferin A isolated from "Indian winter cherry". *Mol Pharmacol* **71**, 426-437 (2007).
11. Menendez-Benito, V., Verhoef, L.G., Masucci, M.G. & Dantuma, N.P. Endoplasmic reticulum stress compromises the ubiquitin-proteasome system. *Hum Mol Genet* **14**, 2787-2799 (2005).
12. Mimnaugh, E.G., Chen, H.Y., Davie, J.R., Celis, J.E. & Neckers, L. Rapid deubiquitination of nucleosomal histones in human tumor cells caused by proteasome inhibitors and stress response inducers: effects on replication, transcription, translation, and the cellular stress response. *Biochemistry* **36**, 14418-14429 (1997).
13. Sheaff, R.J.*, et al.* Proteasomal turnover of p21Cip1 does not require p21Cip1 ubiquitination. *Mol Cell* **5**, 403-410 (2000).
14. Pagano, M.*, et al.* Role of the ubiquitin-proteasome pathway in regulating abundance of the cyclin-dependent kinase inhibitor p27. *Science* **269**, 682-685 (1995).
15. Maki, C.G., Huibregtse, J.M. & Howley, P.M. In vivo ubiquitination and proteasome-mediated degradation of p53(1). *Cancer Res* **56**, 2649-2654 (1996).
16. Rosenberg-Hasson, Y., Bercovich, Z., Ciechanover, A. & Kahana, C. Degradation of ornithine decarboxylase in mammalian cells is ATP dependent but ubiquitin independent. *Eur J Biochem* **185**, 469-474 (1989).
17. Shieh, S.Y., Ikeda, M., Taya, Y. & Prives, C. DNA damage-induced phosphorylation of p53 alleviates inhibition by MDM2. *Cell* **91**, 325-334 (1997).

18. Rogakou, E.P., Pilch, D.R., Orr, A.H., Ivanova, V.S. & Bonner, W.M. DNA double-stranded breaks induce histone H2AX phosphorylation on serine 139. *J Biol Chem* **273**, 5858-5868 (1998).
19. Ling, X., Calinski, D., Chanan-Khan, A.A., Zhou, M. & Li, F. Cancer cell sensitivity to bortezomib is associated with survivin expression and p53 status but not cancer cell types. *J Exp Clin Cancer Res* **29**, 8 (2010).
20. Paoluzzi, L.*, et al.* The BH3-only mimetic ABT-737 synergizes the antineoplastic activity of proteasome inhibitors in lymphoid malignancies. *Blood* **112**, 2906-2916 (2008).
21. Mullally, J.E. & Fitzpatrick, F.A. Pharmacophore model for novel inhibitors of ubiquitin isopeptidases that induce p53-independent cell death. *Mol Pharmacol* **62**, 351-358 (2002).
22. Guterman, A. & Glickman, M.H. Complementary roles for Rpn11 and Ubp6 in deubiquitination and proteolysis by the proteasome. *J Biol Chem* **279**, 1729-1738 (2004).
23. Borodovsky, A.*, et al.* A novel active site-directed probe specific for deubiquitylating enzymes reveals proteasome association of USP14. *EMBO J* **20**, 5187-5196 (2001).
24. Lam, Y.A., DeMartino, G.N., Pickart, C.M. & Cohen, R.E. Specificity of the ubiquitin isopeptidase in the PA700 regulatory complex of 26 S proteasomes. *J Biol Chem* **272**, 28438-28446 (1997).
25. Verma, R.*, et al.* Role of Rpn11 metalloprotease in deubiquitination and degradation by the 26S proteasome. *Science* **298**, 611-615 (2002).
26. Yao, T. & Cohen, R.E. A cryptic protease couples deubiquitination and degradation by the proteasome. *Nature* **419**, 403-407 (2002).
27. Kramer, G.*, et al.* Differentiation between cell death modes using measurements of different soluble forms of extracellular cytokeratin 18. *Cancer Res* **64**, 1751-1756 (2004).
28. Olofsson, M.H.*, et al.* Specific demonstration of drug-induced tumour cell apoptosis in human xenografts models using a plasma biomarker. *Cancer Biomarkers* **5**, 117-125 (2009).
29. Reyes-Turcu, F.E., Ventii, K.H. & Wilkinson, K.D. Regulation and cellular roles of ubiquitin-specific deubiquitinating enzymes. *Annu Rev Biochem* **78**, 363-397 (2009).
30. Lee, B.H.*, et al.* Enhancement of proteasome activity by a small-molecule inhibitor of USP14. *Nature* **467**, 179-184 (2010).
31. Koulich, E., Li, X. & DeMartino, G.N. Relative structural and functional roles of multiple deubiquitylating proteins associated with mammalian 26S proteasome. *Mol Biol Cell* **19**, 1072-1082 (2008).
32. Dimmock, J.R.*, et al.* A conformational and structure-activity relationship study of cytotoxic 3,5-bis(arylidene)-4-piperidones and related N-acryloyl analogues. *J Med Chem* **44**, 586-593 (2001).

Online Methods

Drugs. We obtained b-AP15 (NSC687852) [32] from the Developmental Therapeutics Program of the US National Cancer Institute (http://www.dtp.nci.nih.gov) or from OncoTargeting AB (Uppsala, Sweden). We obtained bortezomib was obtained from the Department of Oncology, Karolinska Hospital. For *in vivo* administration of b-AP15 we dissolved the drug in Cremphor EL:PEG 400 (1:1) by heating to give a working concentration of 2 mg/ml. Working stock was 1:10 diluted in 0.9% normal saline immediately prior to injection.

Connectivity Map analysis. We performed the microarray based gene expression analysis and the Connectivity Map (CMAP) essentially as described [6]. Briefly, MCF7 cells were exposed to 1 mM b-AP15 for 6 h or vehicle (0.1 % DMSO, 6 h). RNA was isolated (RNeasy miniprep kit, Qiagen) followed by quality control, labeling and hybridization to Genome U133 Plus 2.0 arrays (Affymetrix Inc). Raw data was normalized using Mas5 (Affymetrix Inc.) and rank ordered. The following criteria for selection of the 30 most induced (up tags) and the 30 most suppressed (down tags) transcripts were used. Up tags: present call and expression over 300 arbitrary units in the b-AP15 experiment. Down tags: present call after both b-AP15 and vehicle treatment, and expression over 300 arbitrary units in the vehicle experiment. Only tags (i.e. probes) present on HG U133A arrays were used for CMAP compatibility. We have deposited raw and normalized expression data at Gene Expression Omnibus (http://www.ncbi.nlm.nih.gov/geo/) with accession number GSE24150.

Proteasome Inhibition assays. We performed *in vitro* proteasome activity assays using 20S CP (2 nM) in reaction buffer (25 mM Hepes, 0.5 mM EDTA, 0.03 % SDS) or 26S proteasomes in reaction buffer (25 mM Hepes, 50 mM NaCl, 10 mM $MgCl_2$, 2 mM ATP, 1 mM DTT). We used 10 μM Suc-LLVY-AMC, Z-LLE-AMC or Boc-LRR-AMC for the detection of chymotrypsin-like, caspase-like and trypsin-like activity respectively using Wallac Multilabel counter equipped with 380 nm excitation and 460 nm emission filters.

DUB inhibition assays. For DUB inhibition assays we incubated 19S RP (5 nM), 26S (5 nM) UCH-L1 (5 nM), UCH-L3 (0.3 nM), $USP2_{CD}$ (5 nM) $USP7_{CD}$ (5 nM)

$USP8_{CD}$ (5 nM) or BAP1 (5 nM) with DMSO or b-AP15 and monitored cleavage of ubiquitin-AMC (1000 nM) using Wallac Multilabel counter or Tecan Infinite M1000 equipped with 380 nm excitation and 460 nm emission filters.

***In vivo* tumor experiments.** For the *squamous carcinoma* model we subcutaneously injected 1×10^6 FaDu cells into the right rear flank of female SCID mice. We measured tumor growth by the formula $L \times W^2 \times 0.44$. When tumors had grown to a size of approximately 200 mm^3 (Day 0) mice we randomized mice to receive either vehicle (*n*=10) or b-AP15 5 mg kg^{-1} by daily subcutaneous injection s.c. (*n*=15). For the *colon carcinoma* model, we subcutaneously injected 2.5×10^6 *Bcl-2* over-expressing HCT-116 colon carcinoma into the right flank of female nude mice. We treated mice with 5 mg kg^{-1} b-AP15 by intra peritoneal injection (i.p.). For the *lung carcinoma* model we subcutaneously injected 2×10^5 Lewis Lung Carcinoma (LLC) cells into the right rear flank of female C57/B6 mice. When tumors had grown to a size of approximately 50 mm^3 (Day 0) we randomized mice to receive either vehicle (n=4) or b-AP15 5 mg kg^{-1} i.p. (*n*=4) with a treatment cycle consisting of two days treatment followed by two days rest (2 days on/2 days off) for two weeks. For the *breast carcinoma* model we subcutaneously injected 1×10^5 4TD cells into the right mammary fat pad of female BALB/c mice. When tumors had grown to a size approximately 25 mm^3 (d 0), we randomized mice to receive either vehicle (*n*=5) or b-AP15 2.5 mg/kg^{-1} i.p. (*n*=5) with a treatment cycle consisting of one day treatment followed by three days rest (1 day on/3 day off) for 3 weeks. In the *AML* studies we intra venously injected 5×10^5 C1498 AML cells into the tail vein of female C57BL/6J mice. After eight days mice we randomized mice to receive either b-AP15 5 mg kg^{-1} (*n*=10) or vehicle (*n*=10) i.p. for 7 days (d 8 to d 14). Nineteen days after malignant cell injection we sacrificed all mice and evaluated histopathological manifestations of liver and ovary (target organs for this model of tumor) between groups. We conducted all animal experiments in full accordance with Swedish governmental and European statutory regulations on animal welfare. Stockholm North ethics committee approved experiments using squamous, lung and breast carcinoma models. Stockholm South ethics committee approved experiments using the AML model. Experiments using the HCT-116 model were approved by the Ethical Committee for Animal Experimentation, Istituto Nazionale dei Tumori di Milano.

Figure 1

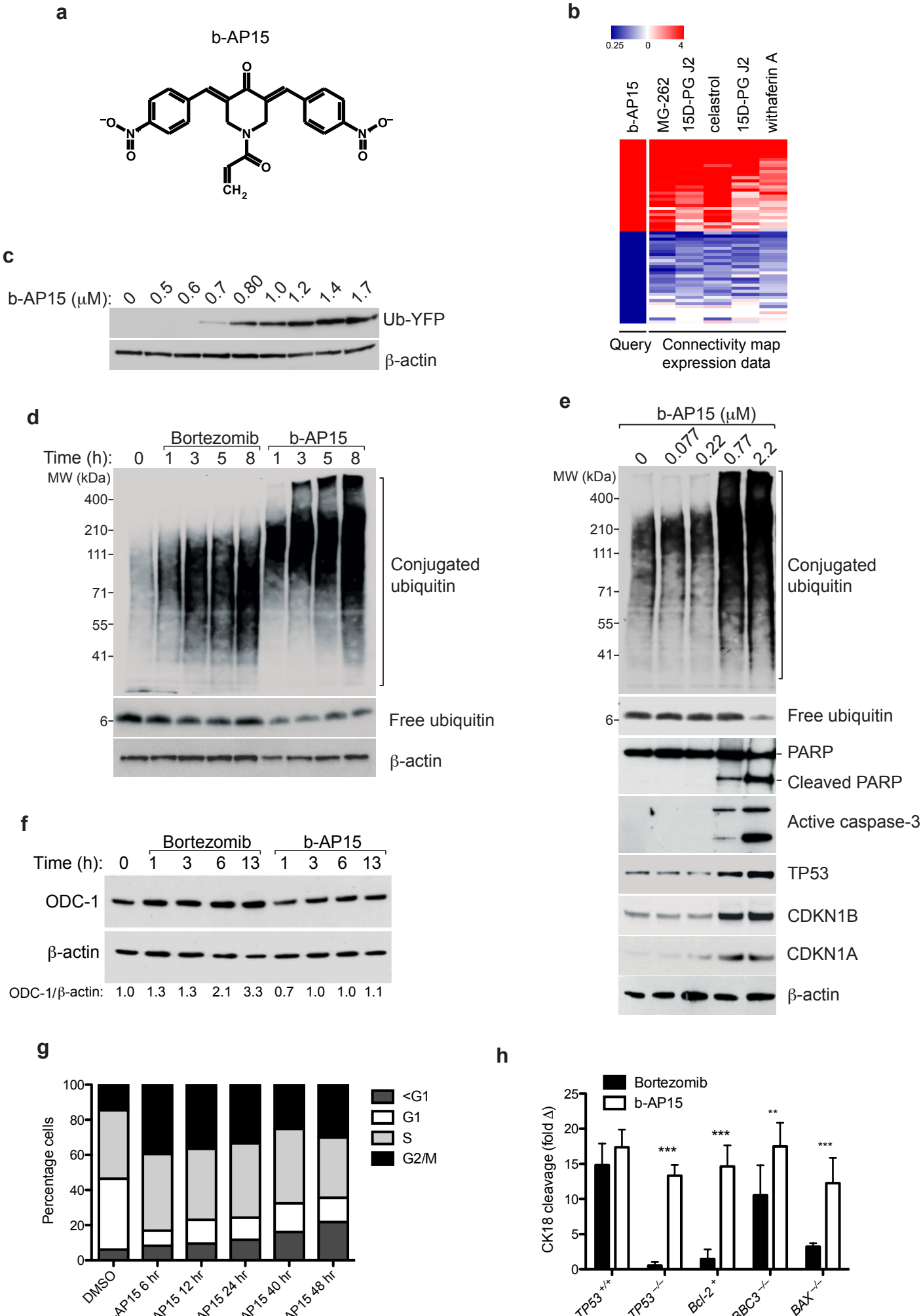
a
b-AP15
b
0.25
0
4
b-AP15
MG-262
15D-PG J2
celastrol
15D-PG J2
withaferin A
Query
Connectivity map
expression data
c
b-AP15 (μM): 0 0.5 0.6 0.7 0.80 1.0 1.2 1.4 1.7
Ub-YFP
β-actin
d
Bortezomib
b-AP15
Time (h): 0 1 3 5 8 1 3 5 8
MW (kDa)
400
210
111
71
55
41
6
Conjugated ubiquitin
Free ubiquitin
β-actin
e
b-AP15 (μM)
0 0.077 0.22 0.77 2.2
MW (kDa)
400
210
111
71
55
41
6
Conjugated ubiquitin
Free ubiquitin
PARP
Cleaved PARP
Active caspase-3
TP53
CDKN1B
CDKN1A
β-actin
f
Bortezomib
b-AP15
Time (h): 0 1 3 6 13 1 3 6 13
ODC-1
β-actin
ODC-1/β-actin: 1.0 1.3 1.3 2.1 3.3 0.7 1.0 1.0 1.1
g
Percentage cells
100
80
60
40
20
0
<G1
G1
S
G2/M
DMSO
b-AP15 6 hr
b-AP15 12 hr
b-AP15 24 hr
b-AP15 40 hr
b-AP15 48 hr
h
Bortezomib
b-AP15
CK18 cleavage (fold Δ)
25
20
15
10
5
0
***
***
**
***
TP53+/+
TP53−/−
Bcl-2+
BBC3−/−
BAX−/−

Figure 2

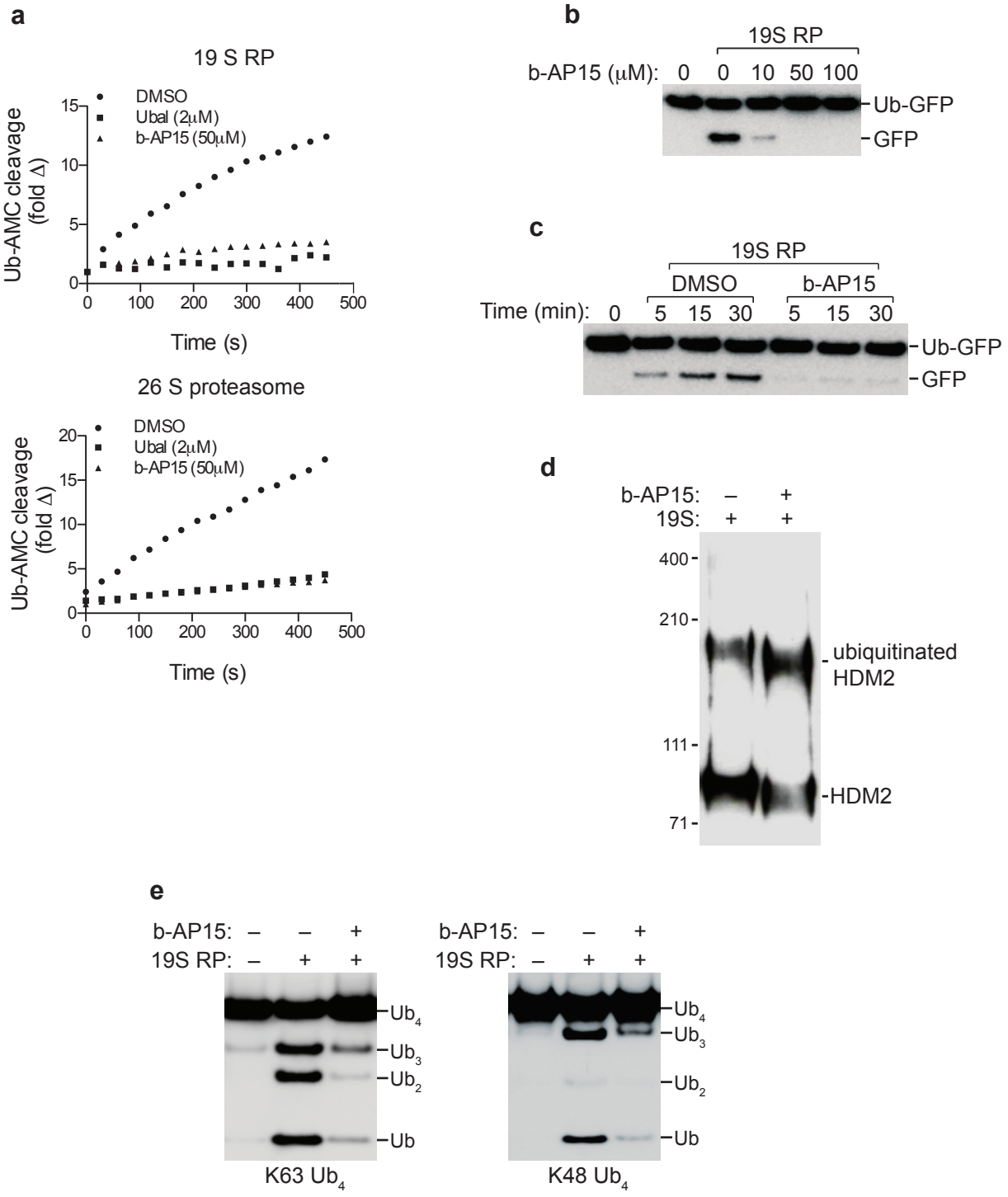
a
19 S RP
DMSO
Ubal (2μM)
b-AP15 (50μM)
Ub-AMC cleavage (fold Δ)
Time (s)
26 S proteasome
DMSO
Ubal (2μM)
b-AP15 (50μM)
Ub-AMC cleavage (fold Δ)
Time (s)
b
19S RP
b-AP15 (μM): 0 0 10 50 100
Ub-GFP
GFP
c
19S RP
DMSO
b-AP15
Time (min): 0 5 15 30 5 15 30
Ub-GFP
GFP
d
b-AP15: – +
19S: + +
400
210
111
71
ubiquitinated HDM2
HDM2
e
b-AP15: – – +
19S RP: – + +
Ub4
Ub3
Ub2
Ub
K63 Ub4
b-AP15: – – +
19S RP: – + +
Ub4
Ub3
Ub2
Ub
K48 Ub4

Figure 3

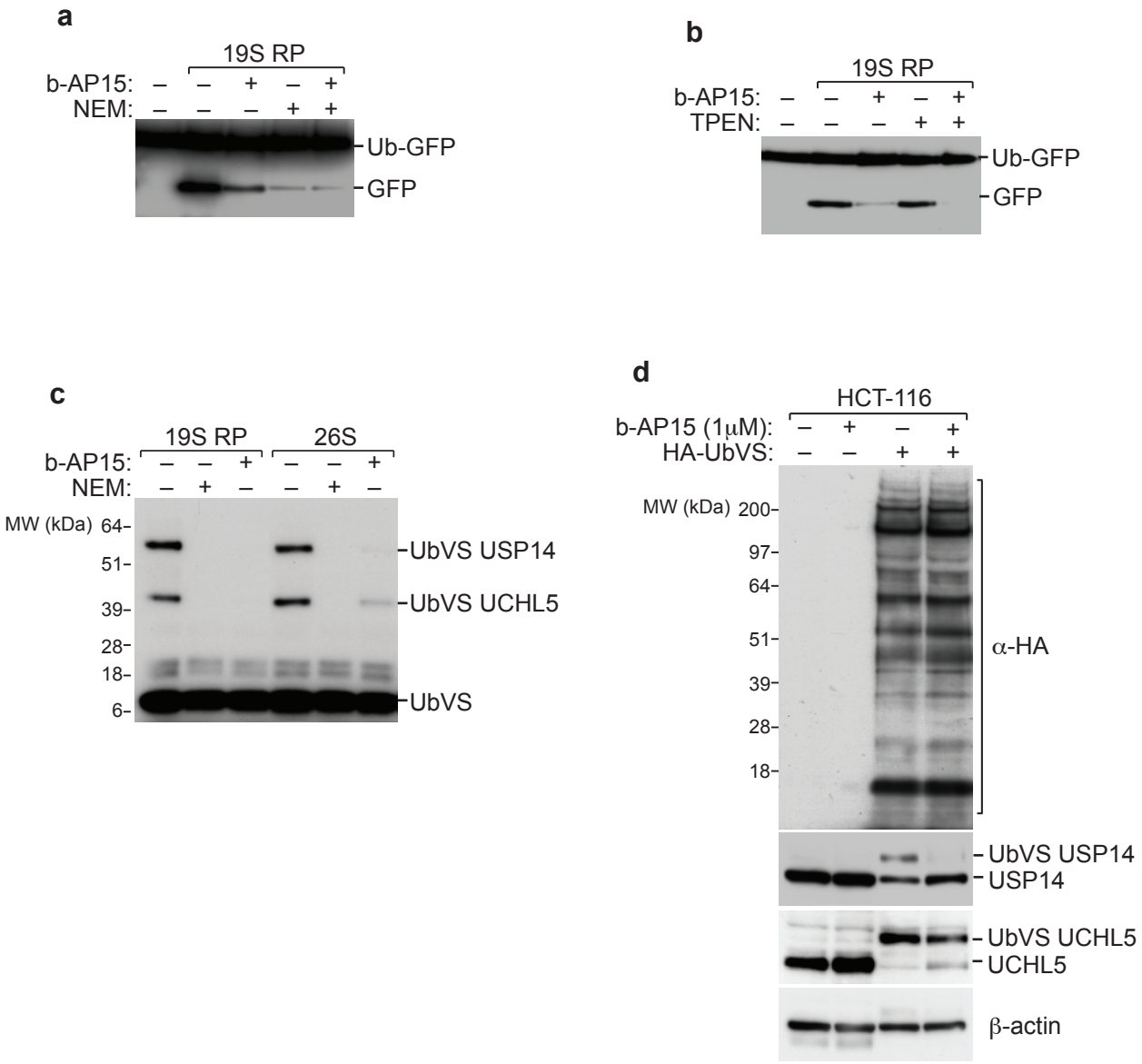
a
19S RP
b-AP15: – – + – +
NEM: – – – + +
Ub-GFP
GFP
b
19S RP
b-AP15: – – + – +
TPEN: – – – + +
Ub-GFP
GFP
c
19S RP
26S
b-AP15: – – + – – +
NEM: – + – – + –
MW (kDa) 64- 51- 39- 28- 18- 6-
UbVS USP14
UbVS UCHL5
UbVS
d
HCT-116
b-AP15 (1μM): – + – +
HA-UbVS: – – + +
MW (kDa) 200- 97- 64- 51- 39- 28- 18-
α-HA
UbVS USP14
USP14
UbVS UCHL5
UCHL5
β-actin

Figure 4

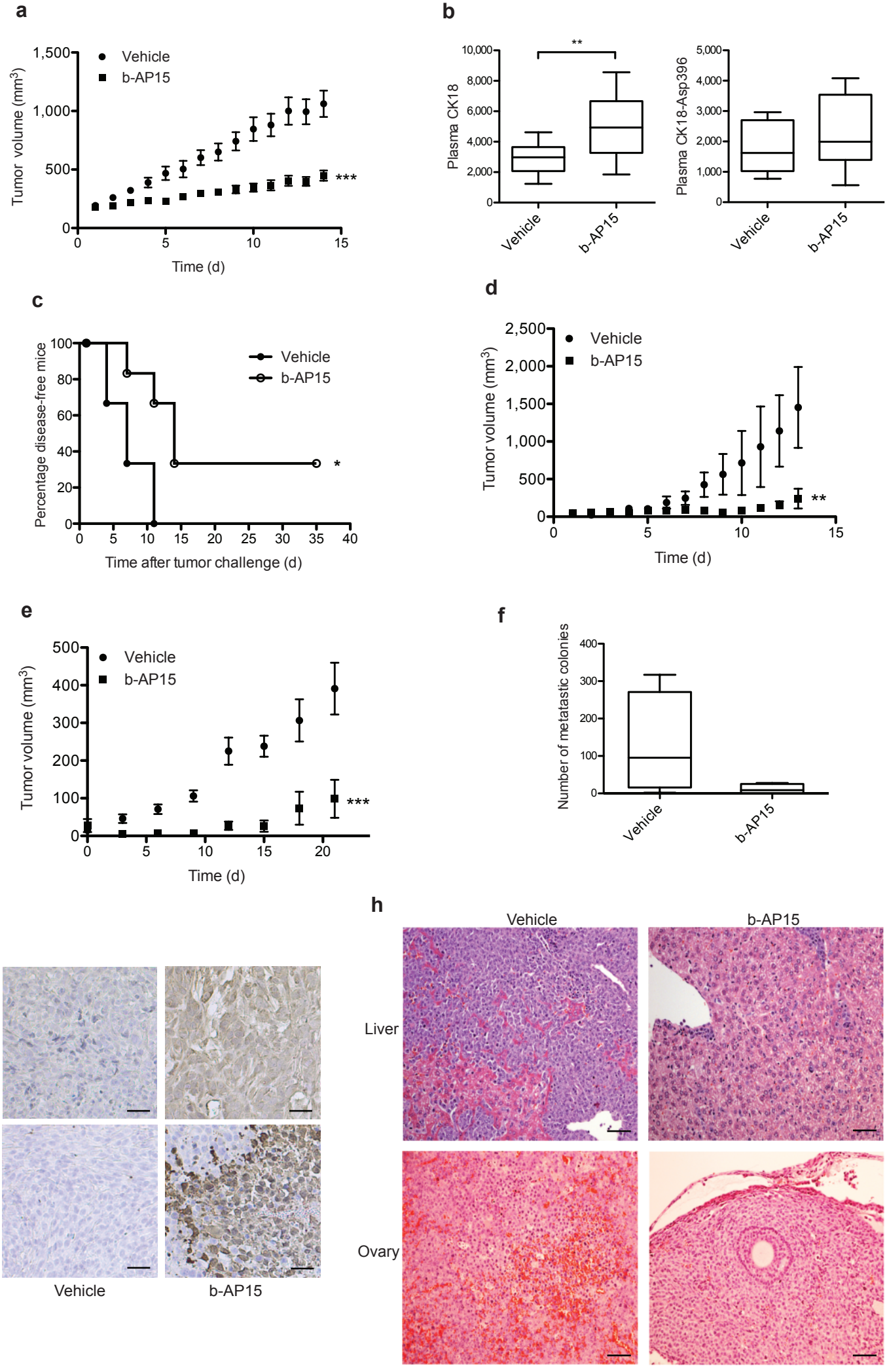
a
Tumor volume (mm3)
Vehicle
b-AP15
Time (d)
***
b
Plasma CK18
Plasma CK18-Asp396
**
Vehicle
b-AP15
c
Percentage disease-free mice
Time after tumor challenge (d)
*
d
Tumor volume (mm3)
Time (d)
**
e
Tumor volume (mm3)
Time (d)
***
f
Number of metatastic colonies
g
K48-linked polyubiquitin
Cleaved Caspase 3
h
Liver
Ovary

Inhibition of proteasome deubiquitinating activity as a novel cancer therapy.

Pádraig D'Arcy, Slavica Brnjic, Maria Hägg Olofsson, Mårten Fryknäs, Kristina Lindsten, Michelandrea De Cesare, Paola Perego, Behnam Sadeghi, Moustapha Hassan, Rolf Larsson and Stig Linder.

Supplementary Figure 1

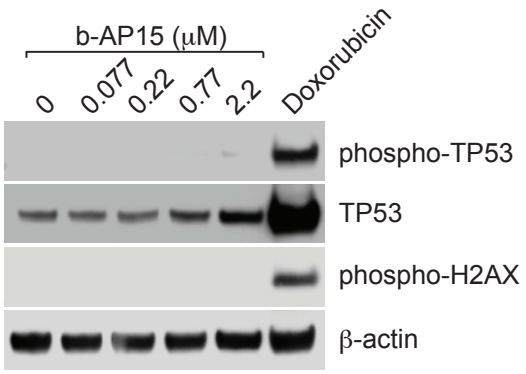

Supplementary Figure 1: b-AP15 does not induce DNA damage.
HCT-116 cells were treated with b-AP15 (1 μM) or doxorubicin (100 nM, as a positive control for genotoxic stress) for 18 h. Cell lysates were immuno-blotted with antibodies for phosphorylated TP53 and histone H2AX as a marker for DNA damage or for total levels of TP53 and β-actin as loading controls.

Supplementary Figure 2

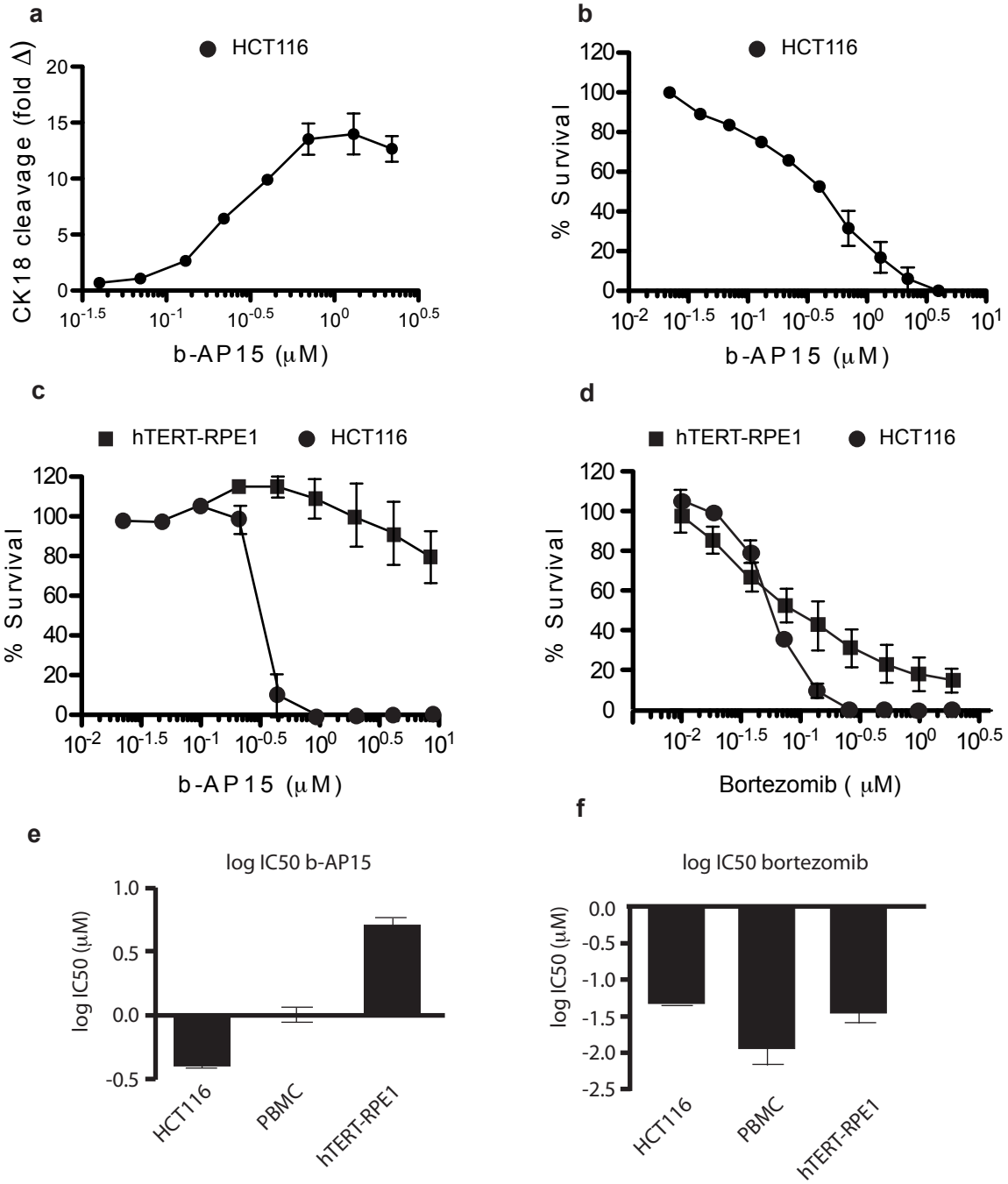

Supplementary Figure 2: b-AP15 induces apoptosis and inhibits cell survival of HCT-116 cells whereas PBMC (periferal blood mononuclear cells) and immortalzied hTERT-RPE1 are less sensitive.

a, HCT-116 cells were treated with increasing concentrations of b-AP15 for 24 h and the levels of apoptosis were determined by measuring the levels of caspase cleaved cytokeratin-18 (CK18) by ELISA assay.

b, HCT-116 cells were treated with increasing concentrations of b-AP15 for 48 h. Cell viability was determined by acid-phosphatase activity assay. Mean values ± s.d. shown.

c, HCT-116 or hTERT-RPE1 cells were treated with increasing concentrations of b-AP15 for 72 hr followed by analysis of cytotoxicity using the FMCA method described.

d, HCT-116 or hTERT-RPE1 cells were treated with increasing concentrations of bortezomib for 72 hr followed by analysis of cytotoxicity using the FMCA method. hTERT-RPE1 is an immortalized human retinal pigment epithelial cell line.

e, f, IC50 was determined from log concentration-effect curves in Graph Pad Prism (GraphPad software Inc., CA, USA) using non-linear regression analysis (four parameter model with variable Hill slope). Concentration-response curves were generated in two-fold dilutions at 8 concentrations of b-AP15 and bortezomib in triplicates using the FMCA assay. The results are expressed as log IC 50 + SD from 4-5 independent experiments (HCT-116, n=5, PBMC (peripheral blood mononuclear cells), n=4, hTERT-RPE1, n=5).

Supplementary Figure 3

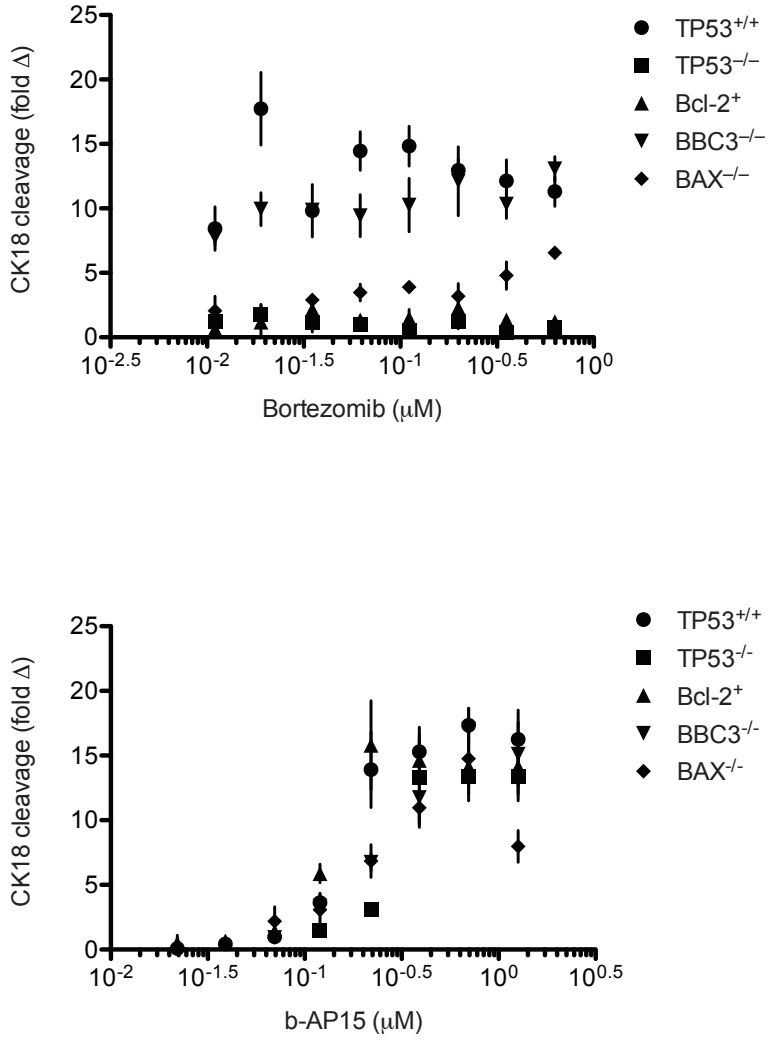

Supplementary Figure 3: Dose response curves of apoptosis induction in isogenic clones of HCT-116 cells.

HCT-116 cells were treated with increasing concentrations of bortezomib or b-AP15 for 24 h and the levels of apoptosis were determined by measuring the levels of caspase cleaved cytokeratin-18 (CK18) by ELISA assay (Mean fold change ± s.d., n=4).

Supplementary Figure 4

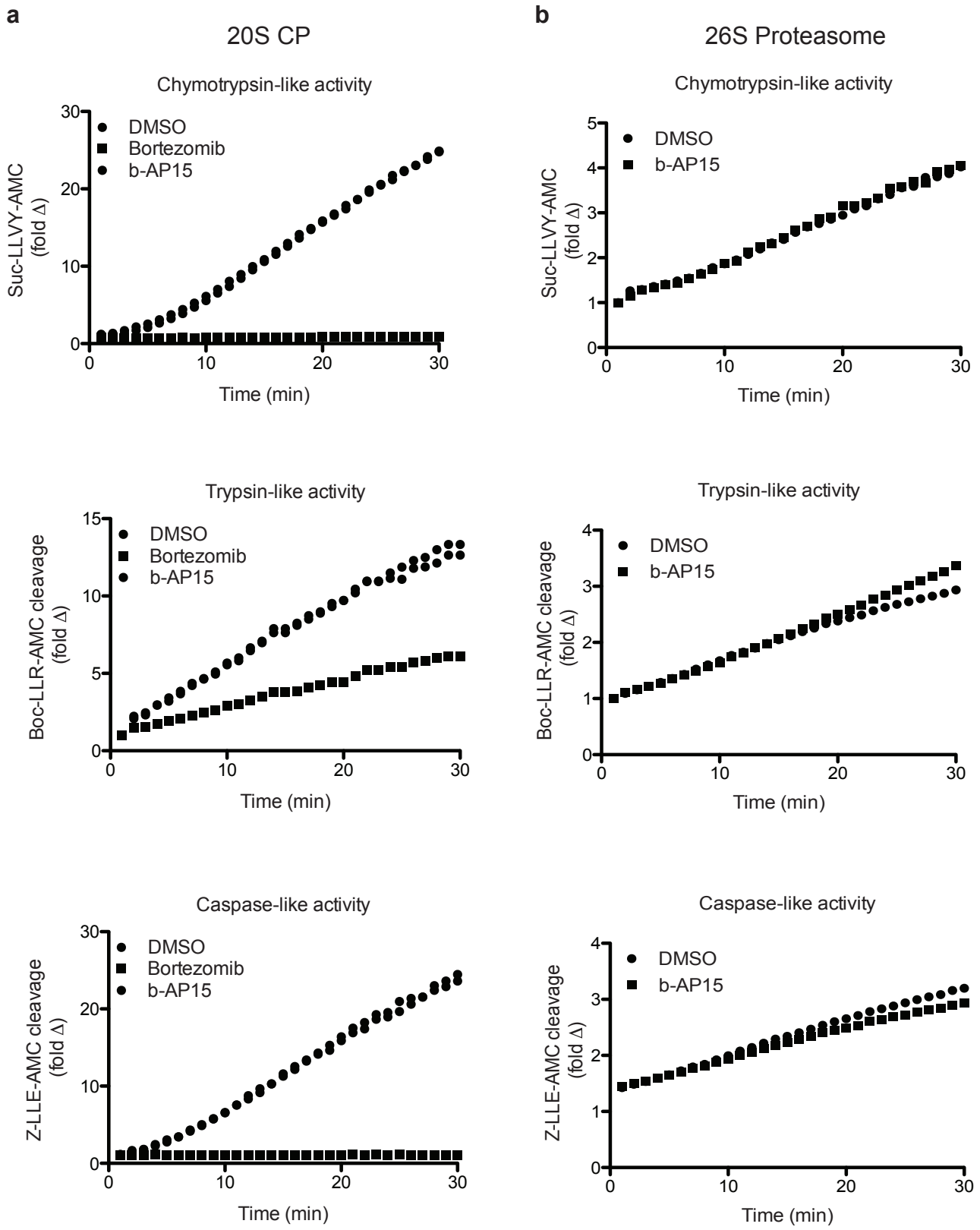

Supplementary Figure 4 : b-AP15 does not inhibit the proteolytic activities of the proteasome.
a, 20S CP (2 nM) were pretreated with DMSO, b-AP15 (50 μM) or bortezomib (100 nM) for 5 min in assay buffer (25 mM HEPES, 0.5 mM EDTA, 0.03% SDS) followed by the addition of 100 μM of the fluorogenic substrates Suc-LLVY-AMC, Z-LLE-AMC or Boc-LRR-AMC for analysis of proteasome chymotrypsin-like, caspase-like and trypsin-like activities respectively.
b, 26S proteasomes (2 nM) in assay buffer (25 mM HEPES, 50 mM NaCl, 10 mM $MgCl_2$, 2 mM ATP, 1 mM DTT) were treated as in **a**. Values represent the fold cleavage in relative fluorescent units.

Supplementary Figure 5

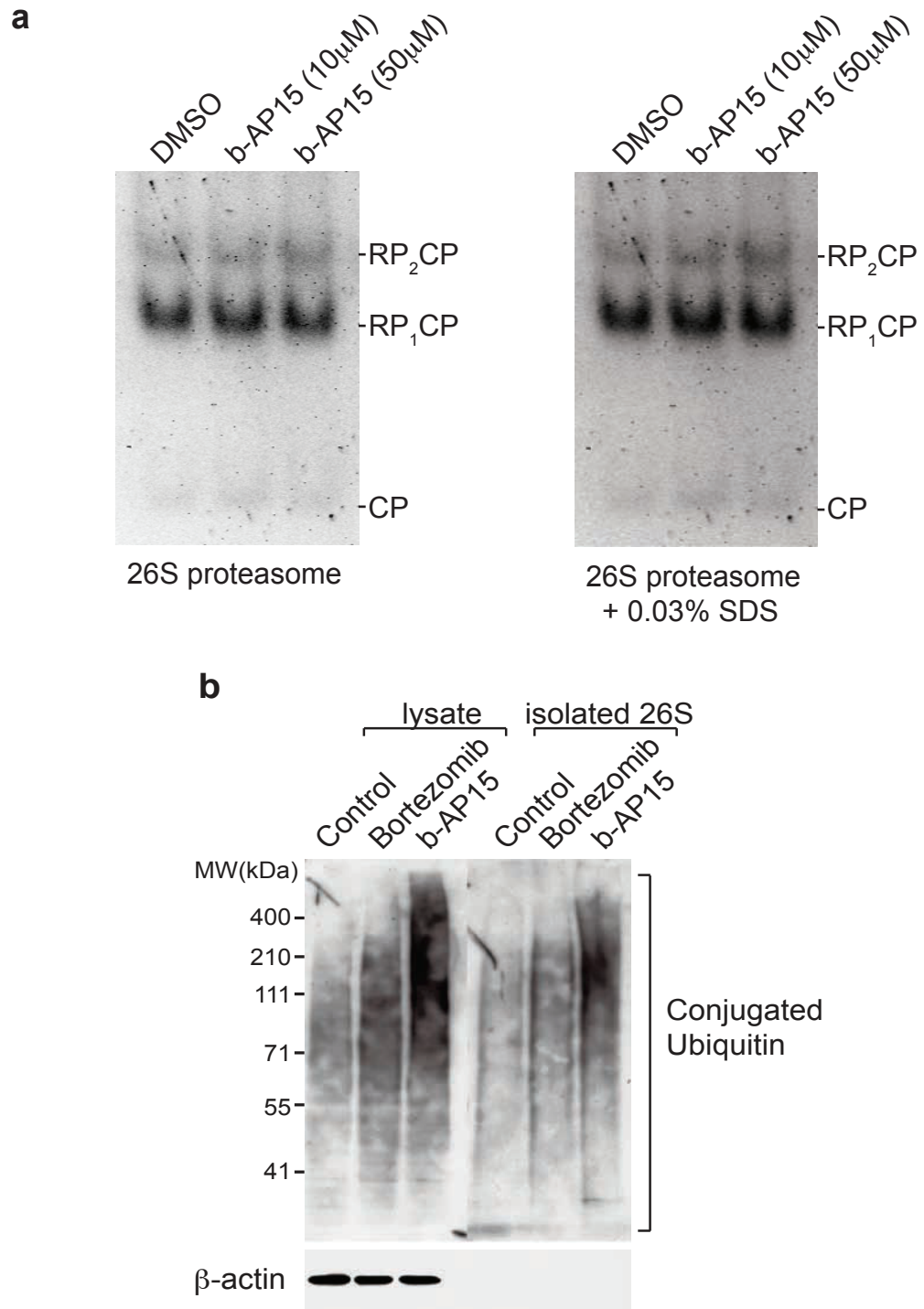

Supplementary Figure 5. b-AP15 does not cause disassociation of 19S and 20S particles or alter ubiquitin binding.

a, Substrate overlay assay of b-AP15 treated proteasomes. Purified 26S proteasome was treated with b-AP15 (10,50 μM) separated by native gel electrophoresis and assayed for proteolytic activity using Suc-LLVY-AMC as a fluorogenic substrate for peptidase activity. Analysis of gels showed the presence of both doubly (RP_2CP) and singly (RP_1CP) capped proteasomes in both control and b-AP15 treated lanes. The addition of 0.03% SDS did not reveal an increase in the presence of uncapped 20S core particles. **b,** b-AP15 does not alter proteasome-ubiquitin binding activity. HCT-116 cells were treated with bortezomib (100 nM) or b-AP15 (1 μM) and proteasomes were affinity purified .The levels of associated polyubiquitin determined by immunoblotting.

Supplementary Figure 6

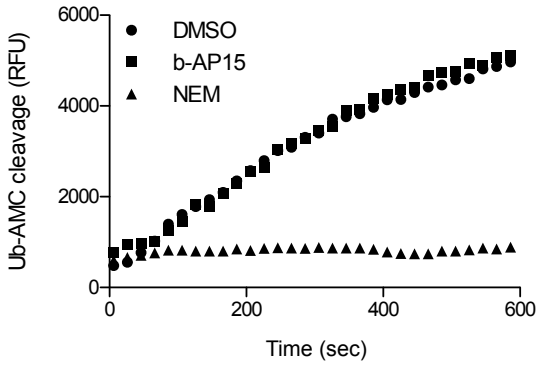

Supplementary Figure 6: b-AP15 does not inhibit total DUB activity.
a, HCT-116 cells were treated for 3 h with b-AP15 (1 μM). Lysates treated with 10 mM N-ethylmaleimide (NEM) were included as a control for total DUB inhibition. DUB activity was determined from cell lysates by measuring the cleavage of the fluorogenic substrate ubiquitin-7-amido-4-methylcoumarin (Ub-AMC).

Supplementary Figure 7

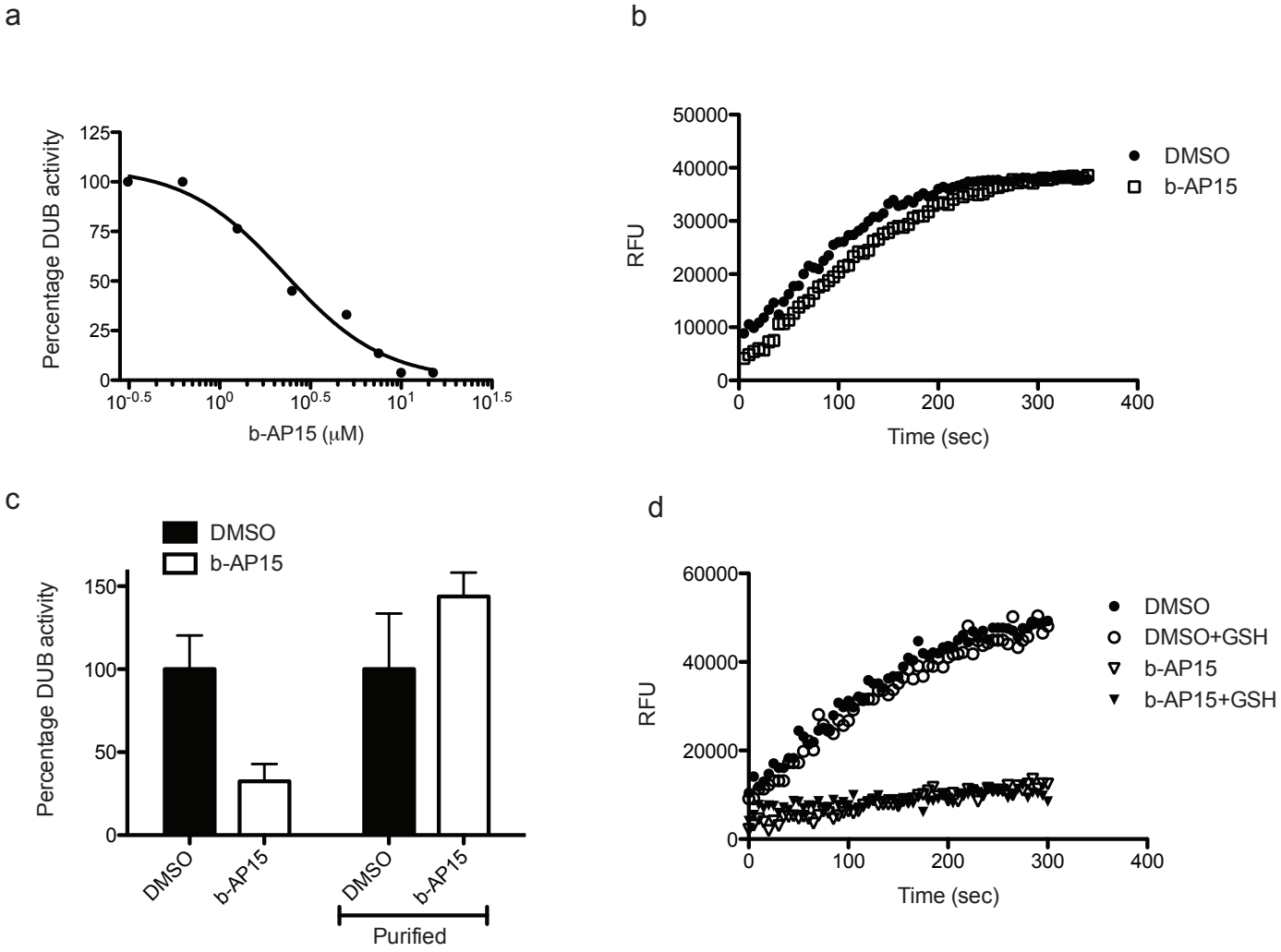

Supplementary Figure 7: **Biochemical characterization of b-AP15 binding**
a, Dose response of b-AP15. Purified 19S proteasomes (5 nM) were treated with indicated concentrations of b-AP15 and DUB activity was determined by detectionof Ub-AMC cleavage. The IC50 value (2.1±0.411 μM) was determined from log concentration curves in Graph Pad Prism using non linear regression analysis. (Mean values ± SD, n=3) .Note that the IC50 observed in cell-free assays is somewhat higher than that observed in cells. A likely explanation to this observation is that the hydrophobicity of b-AP15 (XLogP = 3.3) leads to enrichment of the compound in cells [9].
b, Reversibility of b-AP15 inhibition. The reversibility of inhibition was determined by measuring recovery of 19S DUB activity after rapid dilution of the enzyme b-AP15 complex.
A reaction mix containing 50 time the normal 19S concentration used in reactions (250 nM) and 10 times the calculated IC50 value for b-AP15 (25 μM) was incubated on ice for 15 min followed by a 50 fold dilution in reaction buffer to give a final concentration of 19S 5nM and b-AP15 0.5 μM. The linear reaction curves of Ub-AMC cleavage show that b-AP15 is a reversible inhibitor.
c, Experiment was performed as in **b**, except DMSO and b-AP15 treated proteasomes were purified by spin purification. The recovery of DUB activity after drug removal further suggests that b-AP15 is a reversible inhibitor.
d, To determine if b-AP15 reacts non specifically with cyteine residues 19S (5 nM) was treated with b-AP15 (10μM) or b-AP15 (10 μM) mixed with reduced glutathione GSH (2 mM).
The presence of glutathione did not reduce b-AP15 mediated inhibition of 19S DUB activity.
Cleavage of ubiquitin-AMC was monitored using Tecan Infinite M1000 equipped with 380 nm excitation and 460 nm emission filters.

Supplementary Figure 8

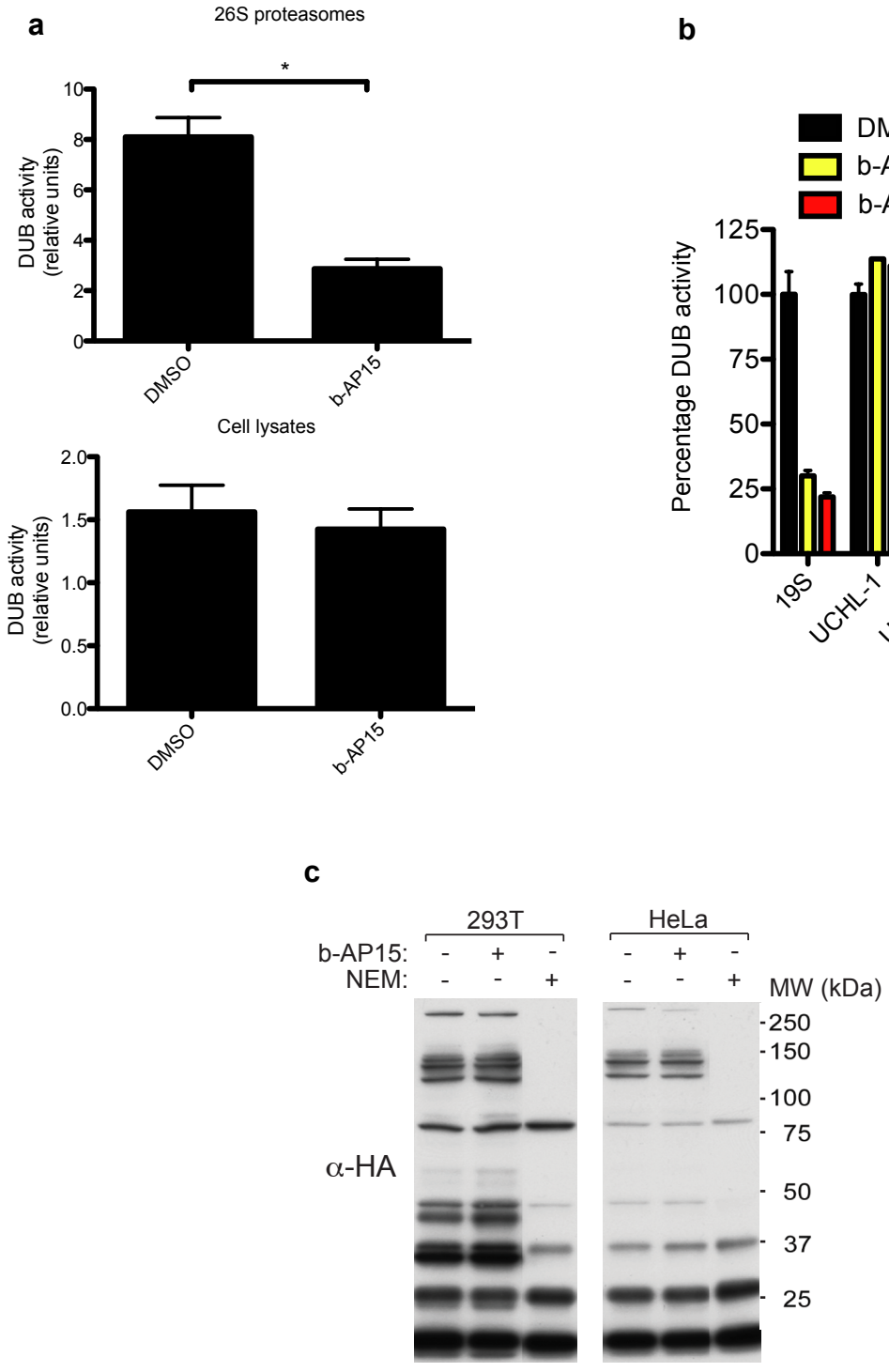

Supplementary Figure 8: b-AP15 is not a general DUB inhibitor.
a, HCT-116 cells were treated with b-AP15 (1 μM) and proteasomes affinity purified. DUB activity of proteasomes is expressed as cleavage of Ub-AMC/suc-LLVY-AMC to normalize for proteasome levels (P=0.012, unpaired t test, two tailed).
b, b-AP15 does not inhibit non proteasomeal DUBs. Recombinant non proteasomal DUBs were treated with b-AP15 as described and percentage activity was determined.
c, Cell lysates from 293T or HeLa cells were treated with b-AP15 (50 μM) followed by active labelling with HA-UbVS. All samples were run on SD-PAGE gels followed by immunoblotting with α-HA antibodies.

Supplementary Figure 9

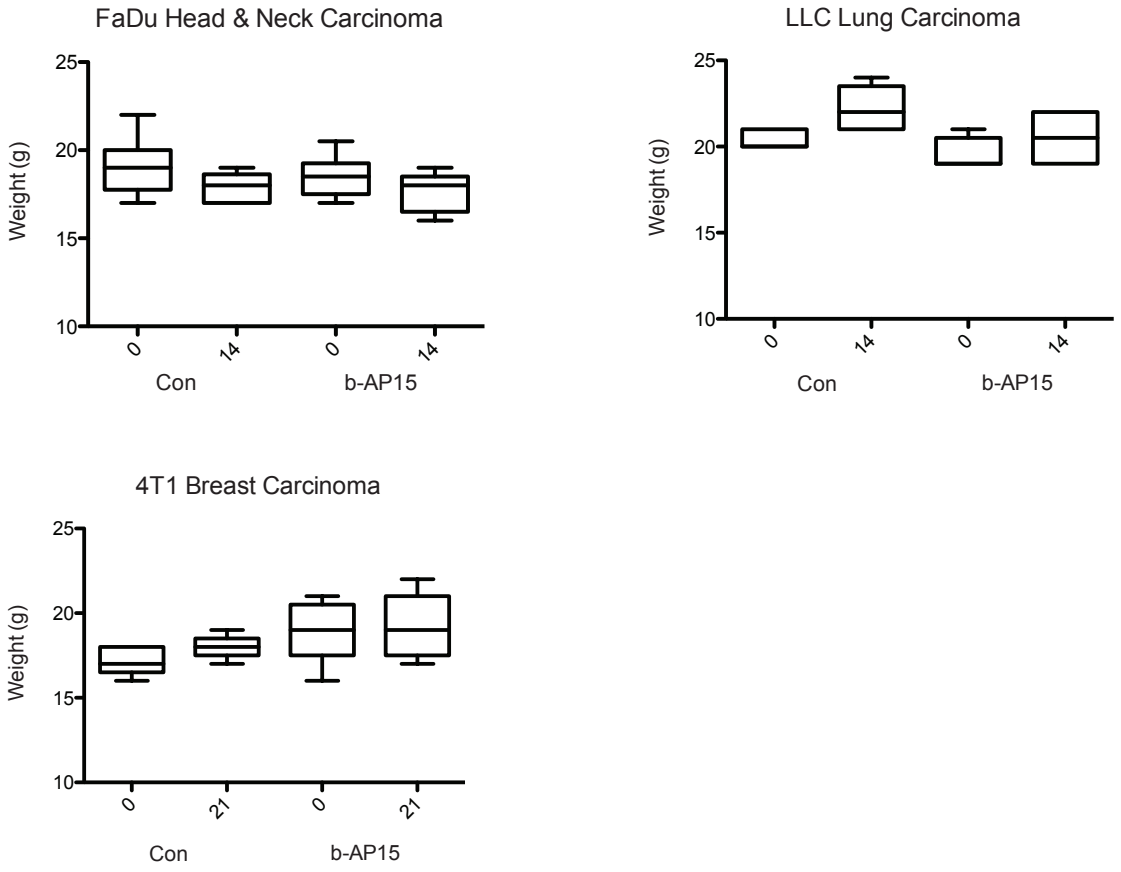

Supplementary Figure 9: b-AP15 treatment does not significantly alter animal weight. The difference in weight at the start and endpoint between control and treated animals for the xenografts presented in Fig. 4 was; FaDu, decrease of 1.3%; LLC, increase 2.1% and 4T1, increase of 5.8 %. Boxes represent the upper and lower quartiles and median, whiskers show maximum and minimum values.

Supplementary Figure 10

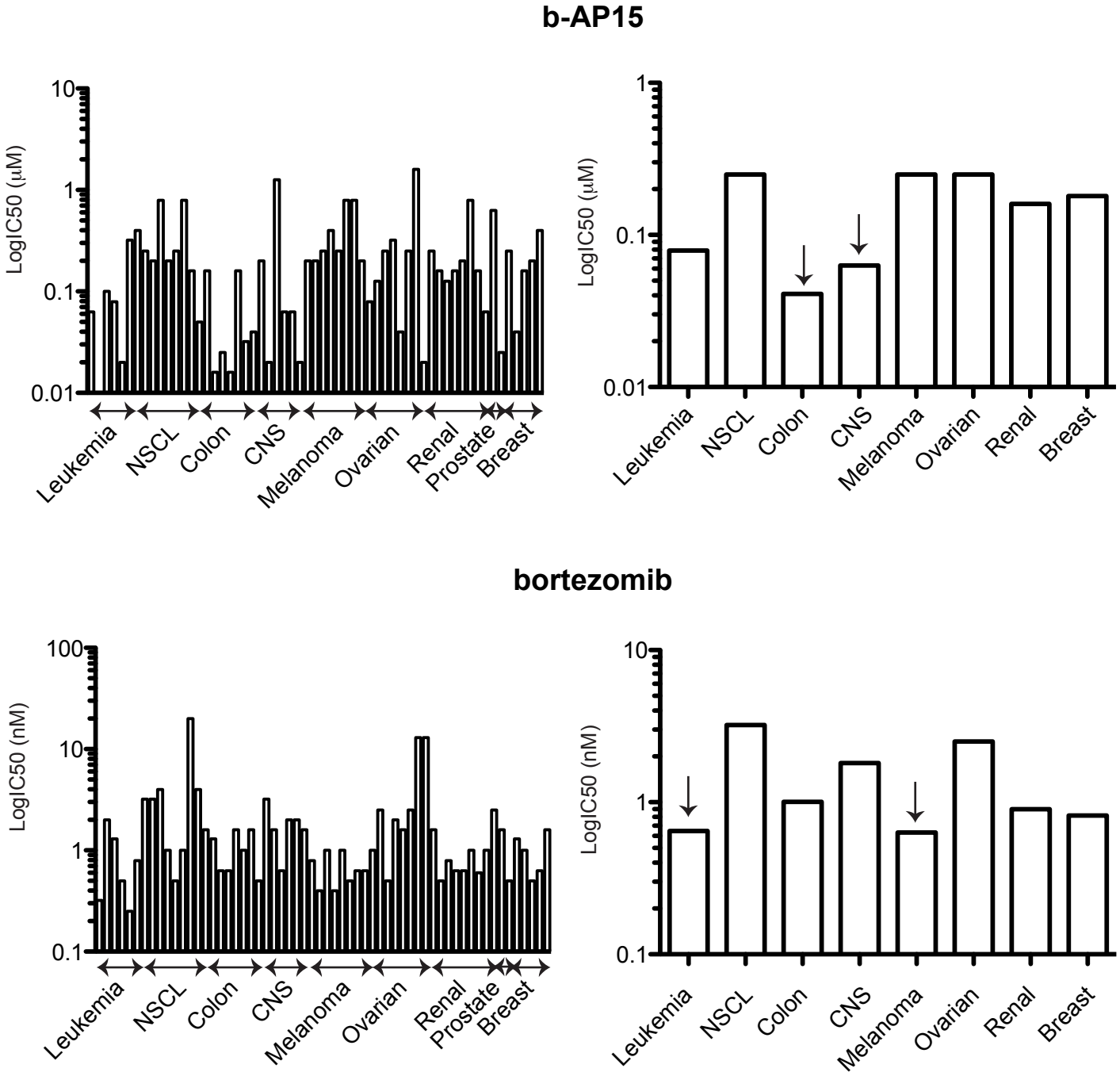

Supplementary Figure 10: Sensitivity of cell lines in the NCI60 panel to b-AP15 and bortezomib. Shown are IC50 values for individual cell lines (left) and median IC50 values for each tumor type (right). Data are from www.dtp.nci.nih.gov. Arrows indicate the two most sensitive tumor cell types for each drug.

Supplementary Table 1. Induction of chaperone expression after b-AP15 treatment

Probe Set ID	Gene Title	Gene Symbol	Expression values		Fold change
			b-AP15	Vehicle	
117_at	heat shock 70kDa protein 6 (HSP70B')	HSPA6	24149	33	725
225061_at	DnaJ (Hsp40) homolog, A4	DNAJA4	21103	711	30
203810_at	DnaJ (Hsp40) homolog, B4	DNAJB4	1955	123	16
205543_at	heat shock 70kDa protein 4-like	HSPA4L	5452	406	13
200666_s_at	DnaJ (Hsp40) homolog, B1	DNAJB1	33900	5251	6
241716_at	heat shock 60kDa protein 1	HSPD1	487	77	6
203811_s_at	DnaJ (Hsp40) homolog, B4	DNAJB4	960	178	5
202581_at	heat shock 70kDa protein 1B	HSPA1B	31068	6382	5
206976_s_at	heat shock 105kDa/110kDa protein 1	HSPH1	40974	8427	5
211016_x_at	heat shock 70kDa protein 4	HSPA4	1803	422	4
202843_at	DnaJ (Hsp40) homolog, B9	DNAJB9	1879	449	4
200880_at	DnaJ (Hsp40) homolog, A1	DNAJA1	19970	4872	4
200800_s_at	heat shock 70kDa protein 1A	HSPA1A	57478	14352	4

Supplementary Table 2. Quantitation of chaperone gene induction.

Gene Title	Gene Symbol	Fold induction[#]	
		b-AP15	bortezomib
heat shock 70kDa protein 6 (Hsp70B')	HSPA6	1550	60
heat shock 70kDa protein 1B (Hspa1b)	HSPA1B	21	12
DnaJ homolog, B1 (Hsp40B1)	DNAJB1	22	5

HCT116 cells were treated with IC90 concentrations of b - AP15 or bortezomib and mRNA levels were determined after reverse transcription and real time PCR. Fold induction is expressed as fold untreated control. The experiment was repeated with similar results.

Supplementary Methods

Reagents. We obtained all reagents from the following sources: 20S proteasome (E-360), 26S proteasome (E-365), 19S proteasome (E-366), Suc-LLVY-AMC (S-280), Z-LLE-AMC (S-230), Boc-LRR-AMC (S-300), Ubiquitin-AMC (U-550), Tetra-ubiquitin K63 (UC-310), Tetra-ubiquitin K48 (UC-210), deconjugating enzyme set (KE10), HA-Ubiquitin Vinyl Sulfone (U-212) (Boston Biochem); anti-β actin (AC-15), ODC-1 (HPA001536) (Sigma Aldrich); anti-LC-3 (2775), anti-GAPDH (2118), anti-p44/42 MAPK (4695), anti-Phospho-p44/42 MAPK (9101)(Cell Signaling); N-Ethylmaleimide (34115) (EMD Chemicals); anti-Ubiquitin K48 (Apu2), anti-Ubiquitin (MAB1510) (Millipore); anti-p53 (DO1), anti-UCHL5 (H-110), Hdm2 (SMP14) (Santa Cruz); anti PARP (C2-10), anti-p27 (G173-524), anti-active Caspase 3 (C92-605) (BD Biosciences); anti-USP14 (A300-919A) (Bethyl Laboratories); anti-HA (12CA5)(Roche).

Cell culture. MCF7 cells were maintained in MEM/10% fetal calf serum. HCT-116 $p53^{+/+}$, $p53^{-/-}$, $Bcl\text{-}2^{+}$, $BBC3^{-/-}$ and $BAX^{-/-}$ cells were maintained in McCoy´s 5A modified medium/10% fetal calf serum. The HCT-116 $p53^{+/+}$ $p53^{-/-}$, $BBC3^{-/-}$ and $BAX^{-/-}$ cells were generated as described [1]. We generated the HCT-116 $Bcl\text{-}2^{+}$ cell line by transfecting parental HCT-116 $p53^{+/+}$cells with pCEP4 *Bcl-2* (Addgene plasmid 16461) [2] and isolating high expression clones . FaDu and LLC3 cells were maintained in DMEM high glucose medium supplemented with 10% fetal calf serum, Na pyruvate, Hepes and non-essential amino acids. 4T1.12B carcinoma cells were maintained in RPMI medium supplemented with 10% fetal calf serum. The proteasome reporter cell line MelJuSo Ub-YFP was generated as described [3]. Cells were maintained in Dulbecco's Modified Eagle's Medium/ 10 % fetal calf serum. The retinal epithelial cell line was generated as described [4]. All cells were maintained at 37^{o}C in 5% CO_2.

Determination of cell apoptosis and viability. We seeded cells in 96-well microtiter plates at 10,000 cells per well and incubated overnight. Cells were treated with indicated drug for 24 h. At the end of the incubation period, NP40 was added to the tissue culture medium to 0.1 % and 25 µl of the content of each well was assayed using the M30-Apoptosense® ELISA as previously described [6]. We determined cell

viability by measuring acid phosphatase activity or by FMCA [7]. For the acid phosphatase activity cells were seeded at 5,000 cells per well in 96-well culture plates and incubated for 12 h at 37°C. Compounds were added to the cells in growth media and incubated for 72 h at 37°C. Cells were washed with 200 µl warm PBS. 100 µl of para-nitrophenyl phosphate (pNPP, 2mg/ml) in Na acetate buffer pH 5 (NaAc 0.1 M, 0.1% Triton-X-100) was added per well. Cells were incubated for 2 h after which reaction was stopped by addition of 1N NaOH. Absorbance was measured at 405 nm.

For the FMCA assay cells were seeded in the drug-prepared 384-well plates using the pipetting robot Precision 2000 (Bio-Tek Instruments Inc., Winooski, VT). The plates were incubated for 72 h and then transferred to an integrated HTS SAIGAN Core System consisting of an ORCA robot (Beckman Coulter) with CO_2 incubator (Cytomat 2C, Kendro, Sollentuna, Sweden), dispenser module (Multidrop 384, Titertek, Huntsville, AL), washer module (ELx 405, Bio-Tek Instruments Inc), delidding station, plate holder, barcode reader (Beckman Coulter), liquid handler (Biomek 2000, Beckman Coulter) and a multipurpose reader (FLUOstar Optima, BMG Labtech GmbH, Offenburg, Germany) for automated FMCA. Survival index (SI) is defined as the fluorescence of test wells in percentage of controls with blank values subtracted.

Substrate overlay assays. We performed native gel electrophoresis essentially as described [5]. In brief 4 µg of purified 26S proteasome (Boston Biochem) was mixed with 10 or 50 µM b-AP15 and incubated at 37°C for 10 min. We resolved samples on 4% non-denaturing PAGE and submerged gels in assay buffer (20 mM Tris-HCL, 5 mM $MgCl_2$, 1 mM ATP, 0.1 mM Suc-LLVY-AMC) and visualized proteasomes under UV illumination.

Ubiquitin-cleavage assay. The recombinant Ub-GFP plasmid pet19b Ub-M-GFP was generated as described [23]. We purified recombinant Ub-GFP from BL21 e.coli cells by His affinity purification. For cleavage assays we incubated 19S RP (25 nM) with 10 mM NEM, 250 µM TPEN or 50 µM b-AP15 for 10 min followed by the addition of recombinant Ub-GFP (200 nM). We performed ubiquitin chain disassembly reactions as above except K48- or K63-linked ubiquitin tetramers (50 ng) were substituted for Ub-GFP. We generated the ubiquitinated HDM2 substrate according to

the Boston Biochem protocol (K-200). For the cleavage assay we incubated 19S RP (25 nM) with 50 μM b-AP15 or DMSO for 10 min followed by the addition of ubiquitinated HDM2 (100 nM).

Proteasome isolation: We treated HCT-116 cells with bortezomib (100 nM) or b-AP15 (1 μM) for 3 hours. We lysed in 50 mM HEPES pH 7.4, 250 mM sucrose, 10 mM $MgCl_2$, 2 mM ATP, 1 mM DTT and 0.025 % digitonin. Samples were sonicated briefly followed by incubation on ice and proteasomes were isolated according to manufacturers protocol.

UbVS labeling. We lysed cell pellets from control or treated cells with buffer (50 mM HEPES pH 7.4, 250 mM sucrose, 10 mM $MgCl_2$, 2 mM ATP, 1 mM DTT) on ice for 15 min and removed debris by centrifugation. We labeled 25 μg of protein with 1 μM HA-UbVS for 30 min at 37^{o}C. We resolved samples by SDS-PAGE and performed immunoblotting.

Cell-cycle analysis. For determination of cell cycle HCT-116 cells were treated with b-AP15 or DMSO Cells were harvested by trypsinisation, washed and fixed in 70% ice cold EtOH for 12 h. Cells were re-suspended in staining solution containing propidium iodide (50 μg/ml) and RNAse A (0.5 μg/ml) in PBS. Samples were run on BD FACScalibur. The percentage of cells in each phase of the cell cycle was determined using ModFit software.

Determination of pulmonary metastases. Since the 4T1 cells are resistant to 6-thioguanine, metastases can be determined by culturing homogonized tissue in the presence of 6-thioguanine. For determination of metatastic 4T1 cells the protocol was as described [8]. In brief lungs from treated or untreated animals were homogenized and treated with collagenase and elastase. Cells were grown in the presence of 60 μM 6-thioguanine for 2 weeks and the number of metastatic colonies determined by giemsa staining.

Determination of caspase-cleaved CK18 in mouse plasma. For measurement of the apoptosis-related CK18-Asp396 fragment, 12.5 ml of plasma was collected 24 h after

last treatment and analyzed using the M30 M30-Apoptosense® assay. Each sample was mixed with 0.4 ml of heterophilic blocking reagent (Scantibodies laboratory Inc).

Immunostaining. Tumor sections were de-paraffinised with xylene, rehydrated and then incubated over-night with K-48 ubiquitin or active-caspase 3 (1/500) diluted in 1% (wt/vol) bovine serum albumin and visualized by standard avidin–biotin–peroxidase complex technique (Vector Laboratories). Counterstaining was performed with Mayer's haematoxylin.

Statistical analyses. For comparisons of treatment groups, we performed the unpaired t test (Mann-Whitney), repeated measures ANOVA and Kaplan-Meier survival (Mantel-Cox test). All statistical analyses were performed using GraphPad Prism Software (version 5.0). Statistical significance was achieved when P was less than 0.05.

1. Bunz, F.*, et al.* Requirement for p53 and p21 to sustain G2 arrest after DNA damage. *Science* **282**, 1497-1501 (1998).
2. Pietenpol, J.A.*, et al.* Paradoxical inhibition of solid tumor cell growth by bcl2. *Cancer Res* **54**, 3714-3717 (1994).
3. Menendez-Benito, V., Verhoef, L.G., Masucci, M.G. & Dantuma, N.P. Endoplasmic reticulum stress compromises the ubiquitin-proteasome system. *Hum Mol Genet* **14**, 2787-2799 (2005).
4. Bodnar, A.G.*, et al.* Extension of life-span by introduction of telomerase into normal human cells. *Science* **279**, 349-352 (1998).
5. Elsasser, S., Schmidt, M. & Finley, D. Characterization of the proteasome using native gel electrophoresis. *Methods Enzymol* **398**, 353-363 (2005).
6. Hagg, M.*, et al.* A novel high-through-put assay for screening of pro-apoptotic drugs. *Invest New Drugs* **20**, 253-259 (2002).
7. Lindhagen, E., Nygren, P. & Larsson, R. The fluorometric microculture cytotoxicity assay. *Nat Protoc* **3**, 1364-1369 (2008).
8. Pulaski, B.A. & Ostrand-Rosenberg, S. Mouse 4T1 breast tumor model. *Curr Protoc Immunol* **Chapter 20**, Unit 20 22 (2001).
9. Sawada, G. A. *et al.* Increased lipophilicity and subsequent cell partitioning decrease passive transcellular diffusion of novel, highly lipophilic antioxidants. *J Pharmacol Exp Ther* **288**, 1317-1326 (1999).